The atomic resolution structure of human aldose reductase reveals that rearrangement of a bound ligand allows the opening of the safety-belt loop

Marianna Biadene,[a] **Isabelle Hazemann,**[b]‡ **Alexandra Cousido,**[b] **Steve Ginell,**[c] **Andrzej Joachimiak,**[c] **George M. Sheldrick,**[a] **Alberto Podjarny**[b] **and Thomas R. Schneider**[d,e]*§

[a]Lehrstuhl für Strukturchemie, Georg-August Universität, Tammanstrasse 4, D-37077 Göttingen, Germany, [b]UPR de Biologie Structurale, IGBMC, CNRS INSERM ULP, 1 Rue Laurent Fries, BP 163, 67404 Illkirch, France, [c]Argonne National Laboratory, Argonne, USA, [d]IFOM–The FIRC Institute of Molecular Oncology Foundation, Via Adamello-16, 20139 Milan, Italy, and [e]European Institute of Oncology, Via Ripamonti 435, 20141 Milan, Italy

‡ Present address: IBS, 41 Avenue des Martyrs, Grenoble, France.
§ Present address: EMBL c/o DESY, Notkestrasse 85, 22603 Hamburg, Germany.

Correspondence e-mail: thomas.schneider@embl-hamburg.de

The crystal structure of human aldose reductase in complex with citrate has been determined to a resolution of 0.82 Å. The difference electron density for H atoms unequivocally shows that the cofactor is in the oxidized state corresponding to the situation after the catalytic event has occurred. A citrate molecule bound to the active site has been modelled in two different conformations. These two conformations correlate with a fully closed and a partially open conformation of the so-called safety-belt loop (Gly213–Ser226). The open conformation is observed for the first time with the cofactor bound to the protein and may be related to the initial phase of the opening of the safety belt. The structure suggests that after the catalytic event, a rearrangement of a bound ligand can trigger the opening of the safety-belt loop, thus initiating the release of the oxidized cofactor.

1. Introduction

Human aldose reductase (ALR2; EC 1.1.1.21) is a member of the aldo-ketoreductase superfamily and catalyzes the NADPH-dependent reduction of a wide variety of aldehydes to their corresponding alcohols. Under hyperglycaemic conditions, the enzyme converts glucose to sorbitol. High levels of sorbitol have been connected to diabetic complications such as glaucoma, retinopathies and cataracts (Costantino *et al.*, 1999; Yabe-Nishimura, 1998; Kinoshita & Nishimura, 1988; Dunlop, 2000). Inhibition of aldose reductase as a means of avoiding high levels of sorbitol has thus become an attractive route for the treatment of long-term diabetic complications (Costantino *et al.*, 2000; Petrash, 2004; El-Kabbani, Ruiz *et al.*, 2004; Klebe *et al.*, 2004; Podjarny *et al.*, 2004; Srivastava *et al.*, 2005).

Human aldose reductase consists of 315 residues and folds as an eight-stranded β/α-barrel to which a small β-sheet capping the N-terminal face (residues 2–14) of the barrel and a C-terminal extension (residues 275–315) are added (Fig. 1). The active site is located on the C-terminal side of the barrel. The cofactor NADPH straddles the barrel and contributes its nicotinamide moiety to the active-site machinery (Rondeau *et al.*, 1992; Wilson *et al.*, 1992).

The mechanism for the forward reaction catalyzed by AR can be described as a sequential ordered mechanism (Grimshaw *et al.*, 1990*a*, 1995; Kubiseski *et al.*, 1992) in which NADPH binds first, followed by the binding of the aldehyde substrate. After conversion of the aldehyde into an alcohol, the product of the reaction is released and the oxidized cofactor disengages from the enzyme. Kinetic and spectroscopic experiments have shown that both the uptake and release of the cofactor are accompanied by conformational changes of the enzyme–cofactor complex. In the forward

reaction, an initial isomerization takes place after the binding of the cofactor (Kubiseski *et al.*, 1992), while a second isomerization occurs after the reaction is completed but prior to the release of the cofactor (Grimshaw *et al.*, 1990*b*). Furthermore, kinetic experiments have shown that both the reduced and oxidized version of the cofactor bind very tightly to the enzyme, with K_d values smaller than 100 n*M* (Grimshaw *et al.*, 1990*a*; Kubiseski *et al.*, 1992), and that the conformational change preceding the dissociation of the cofactor is the overall rate-limiting step in the enzymatic cycle (Grimshaw *et al.*, 1995).

In the crystal structure, the cofactor is held in position and sequestered from solvent by residues that are mostly located in the loop between strand and helix 7 of the β/α-barrel (Fig. 1); this loop (residues Gly213–Ser226) has therefore been named the 'safety-belt' loop (Wilson *et al.*, 1992). In a comparison of the crystal structures of a mutated version of human AR (Cys298Ser) in complex with NADP(H) and of porcine AR in complex with ADPRP (Rondeau *et al.*, 1992), Borhani and coworkers found that the conformation of the safety belt depends on the presence of the cofactor in its binding site and suggested that motion of this loop is connected with uptake and release of the cofactor (Borhani *et al.*, 1992) . Recently, Bohren and coworkers introduced a point mutation, Arg268Ala, into human AR that removes an important interaction point between the enzyme and the cofactor, thereby reducing the affinity of NADPH by several orders of magnitude (Bohren *et al.*, 2005). Interestingly, this mutated form of the protein could be crystallized in the absence of the cofactor, providing a realistic picture of the structure of human AR in the apo form. In the crystal struc-ture of apo-R268A AR, the safety belt assumes an open conformation that, owing to a stabilizing π-stacking inter-action between Trp219 and Arg293, can be observed as ordered in the crystal structure (Fig. 2).

In the following, we present the crystal structure of wild-type human AR in complex with its cofactor and citrate at atomic resolution. In this structure, the safety-belt loop can be seen in two alternative conformations: closed and partially opened.

2. Material and methods

2.1. Expression and purification

The open reading frame of the human ALR2 gene (Gene Bank/EMBL Data Bank accession No. J05017) was amplified by PCR from cDNA and cloned into the T7 RNA polymerase-based vector pET15b (Novagene). The expression of hexa-histidine-tagged protein in *Escherichia coli* strain BL21 (DE3) (Novagen) was induced at 310 K using IPTG (Euromedex) during a 3 h period. The pellet from a 4 l culture was disrupted by sonication and centrifugation. The supernatant was loaded onto a Talon metal-affinity column (Clonetech). After thrombin cleavage of the hexahistidine extension, the detagged protein was loaded onto a DEAE Sephadex A-50 column (Pharmacia) and eluted with an NaCl gradient (Lamour *et al.*, 1999).

2.2. Crystallization

Human aldose reductase at a concentration of 16 mg ml^{-1} in 50 m*M* ammonium citrate buffer pH 5 was mixed with
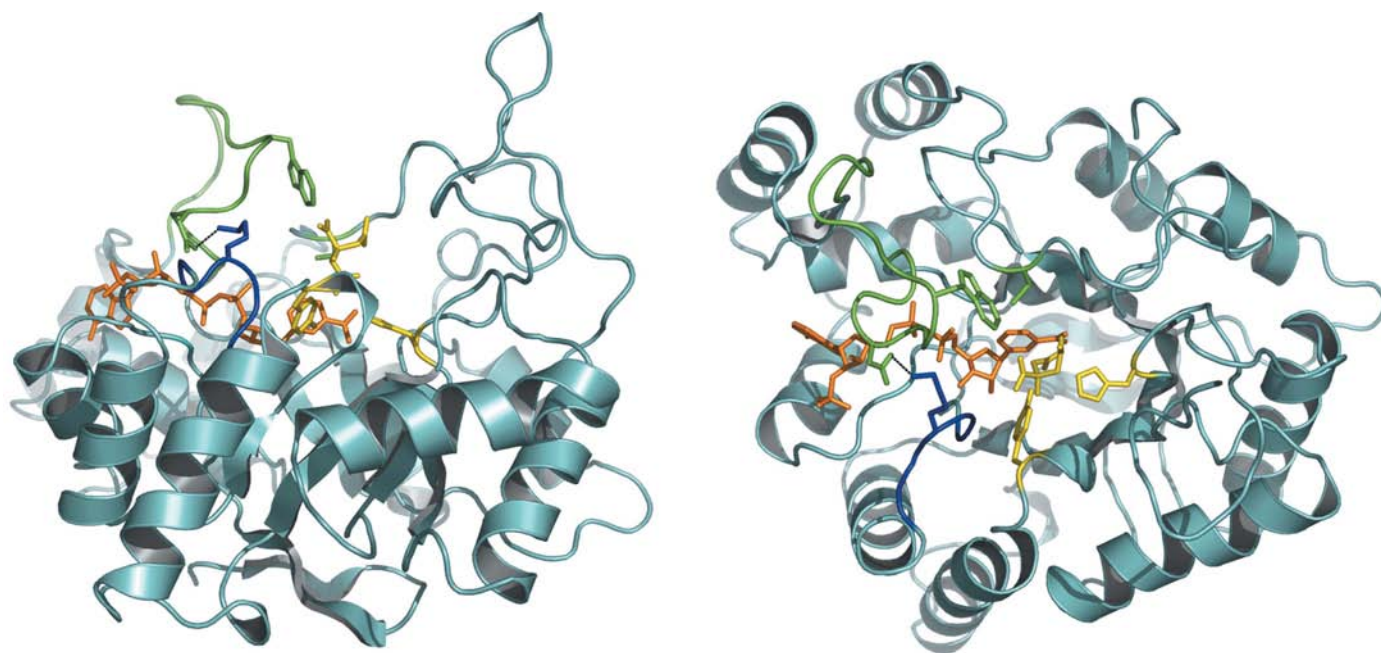

Figure 1
Two views rotated by 90° from each other of the overall structure of human aldose reductase. The safety-belt loop (residues Gly213–Ser226) and Cys298 are shown in green; for Asp216, Trp219 and Cys298 the side chains are depicted. The loop opposing the safety-belt loop (containing residue Lys21, which forms a crucial salt bridge to Asp216 in the closed conformation of the safety-belt loop) is shown in dark blue. The cofactor and the ligand are shown in orange and yellow, respectively. The side chains of Tyr48 and His110 are shown in yellow.

NADP$^+$ and the 2R4R isomer of the inhibitor Fidarestat in a 1:2:2.5 ratio. The hanging-drop vapour-diffusion method was
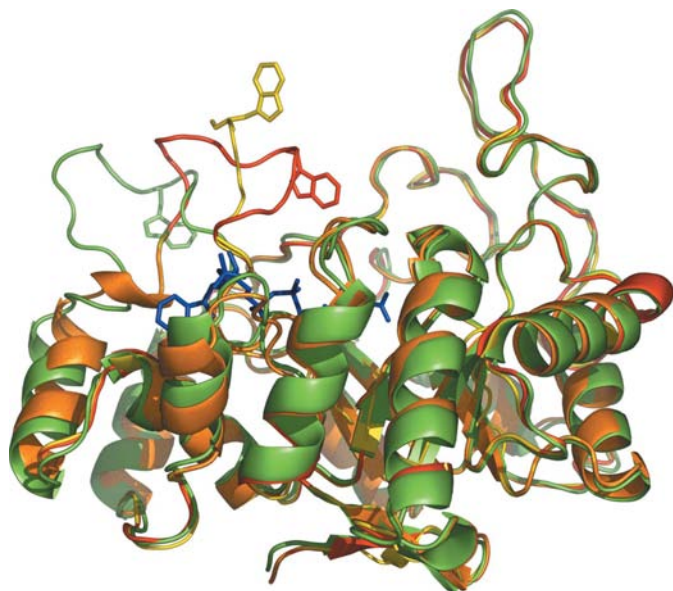

Figure 2
Different conformations of the safety-belt loop. The closed and open conformations of the present model are shown in red and yellow (regions for which both conformers are identical are coloured orange), while the open conformation found in the structure of the R298A mutant apo-AR (PDB code 1xgd) is shown in green. For all conformers the side chain of Trp219 is shown. The cofactor is depicted in blue.
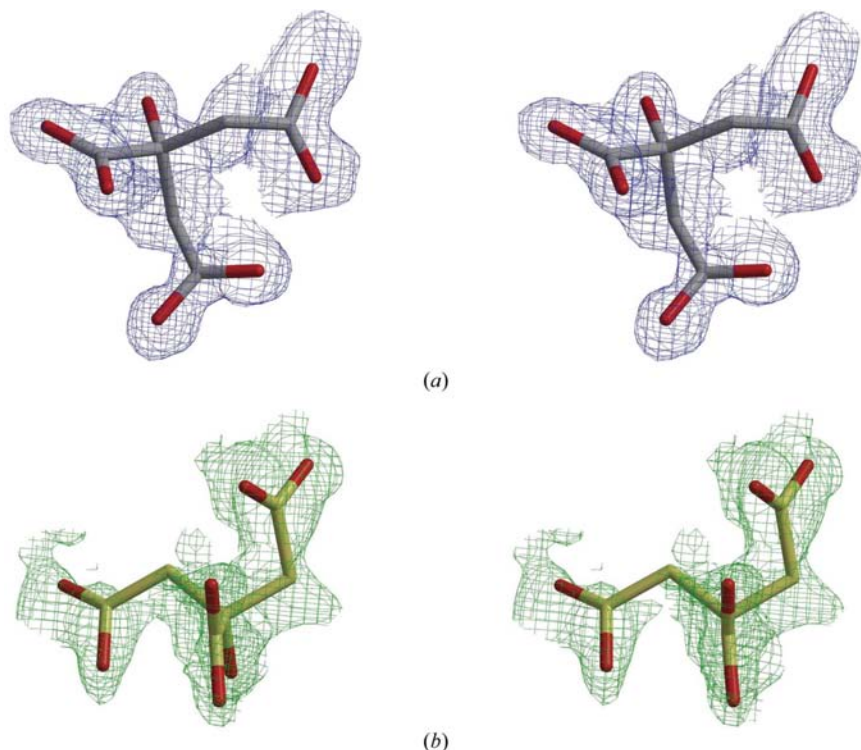

Figure 3
Cross-eyed stereoviews of difference electron density for citrate bound in the active site. (a) σ_A-Weighted $2mF_o - DF_c$ difference electron density contoured at 1σ for the major conformer (63%) of citrate. (b) $F_o - F_c$ difference electron density contoured at 2σ as calculated in the presence of the first conformer of citrate but before adding the minor conformer (37%). The refined position of the minor conformer is shown.

used to crystallize the ternary complex. 5 µl of the solution containing the protein and the cofactor was mixed with an equal volume of 15%(w/v) polyethylene glycol (PEG) 6000 in 50 mM ammonium citrate buffer pH 5. The reservoir solution (1 ml) contained 120 mM ammonium citrate and 20% PEG 6000. Crystals grew at 277 K; prior to data collection, they were transferred into a stabilization solution (25% PEG 6000) and then into a cryoprotecting solution (40% PEG 6000) and were finally frozen in liquid nitrogen.

2.3. Data collection and processing

Diffraction data were collected to 0.82 Å from a single crystal at beamline ID19 at the APS Structural Biology Centre (Rosenbaum *et al.*, 2006) at 10 K (λ = 0.7999 Å) using a MAR CCD detector (MAR Research, Norderstedt, Germany) and an in-house helium-cooling device (Petrova *et al.*, submitted work). To cover the full dynamic range of the diffraction data, two data sets were collected: a low-resolution data set extending to 1.44 Å (676 frames with an oscillation angle of 0.5°) and a high-resolution data set extending to 0.82 Å (1690 frames with an oscillation angle of 0.2°). In the high-resolution data set, systematic changes in refined B values and scale factors between frames 900 and 1690 indicated the onset of radiation damage. Therefore, we only used diffraction intensities from the low-resolution pass and the first 900 frames (corresponding to 180° rotation of the crystal) of the high-resolution pass to construct the merged data set for refinement. The data were integrated and scaled using *DENZO* and *SCALEPACK* (Otwinowski & Minor, 1997). Further data analysis and merging was performed using *XPREP* (Bruker AXS, Madison, USA). 5% of the unique reflections were randomly flagged by *XPREP* for use in cross-validation. Data statistics are shown in Table 1.

2.4. Structure solution, refinement and validation

Initial phases were determined by molecular replacement using the program *EPMR* (Kissinger *et al.*, 1999) against data truncated to 4.0 Å resolution. The crystal structure of human AR in complex with the inhibitor IDD384 determined to 1.7 Å resolution (Calderone *et al.*, 2000) was used as a search model. The best solution found by *EPMR* had a correlation coefficient of 68.9% and a crystallographic R factor of 34.3%. Refinement was performed with *SHELXL*97 (Sheldrick & Schneider, 1997). Visual inspection and manual rebuilding of the model were performed with *XFIT* (McRee, 1999). Water molecules were initially placed automatically with *SHELXWAT*, while in later stages solvent molecules were added and removed manu-

Table 1
Data statistics for human AR in complex with NADP$^+$.

The crystal belonged to space group $P2_1$, with unit-cell parameters a = 47.45, b = 66.76, c = 49.31 Å, $\alpha = \gamma = 90$, $\beta = 91.55°$ as determined by post-refinement with *SCALEPACK* (Otwinowski & Minor, 1997). Values in parentheses are for the highest resolution shell (0.85–0.82 Å).

Resolution range (Å)	34.6–0.82
No. of observations	1276555
No. of unique reflections	282677
Redundancy	4.5 (3.3)
$\langle I/\sigma(I) \rangle$	26.1 (11.8)
Completeness (%)	94.4 (90.4)
R_{int}† (%)	4.2 (8.4)

† $R_{int} = \sum \left| I - \langle I \rangle \right| / \sum I$.

ally. Stereochemical parameters for NADP$^+$ were derived from the model refined by Pavelites *et al.* (1997) and for the citrate molecules the model refined by Rossi *et al.* (1983) was used (CSD entry CADJIA D/B 3497).

Refinement and manual building of models with isotropic B factors against all data (to the resolution limit of 0.82 Å) resulted in an R_{work} of 19.1% and an R_{free} of 21.5%. When the atoms of this model were modelled with anisotropic B factors, R_{work} and R_{free} fell to 14.5% and 15.9%, respectively (corresponding to a fall in R_{free} of 5.6%). In the final stages of refinement, most H atoms were clearly visible in difference electron-density maps; their inclusion at calculated positions using the *SHELXL* riding model reduced R_{work} and R_{free} by 1.2% and 1.3%, respectively.

To describe the electron density in the active site, one citrate molecule was initially placed with its occupancy fixed at a value of 0.7. After several cycles of refinement, a second conformation of the citrate molecule could be localized in $F_o - F_c$ difference electron density (Fig. 3). At convergence, the occupancies of the two conformations were 0.63 and 0.37, with mean B values of 13.7 and 22.5 Å^2, respectively.

To finalize the refinement, the best model obtained from refinement against the working set of reflections only was refined against all data for 20 cycles using conjugate-gradient minimization and an $R1$ of 9.73% was obtained. After the removal of all restraints, the part of the normal matrix corresponding to the coordinates was inverted in order to estimate the standard deviations. For 32 154 parameters and 282 465 reflections, this required 318 MB of memory and took 4.5 h of CPU time on an Intel Xeon (3.0 GHz) based system running under Linux. Refinement statistics are shown in Table 2.

To verify the minor conformation of the safety-belt loop, the occupancies and B values of the sites of the major conformation were fixed at their refined values, while the minor conformation was excluded from the structure-factor calculations. To remove model bias, the modified model was subjected to 20 cycles of conjugant-gradient minimization starting at a resolution of 1.4 Å and including additional resolution shells of 0.1 Å at every cycle of refinement until the maximum resolution of 0.82 Å was reached (*SHELXL* command STIR 1.4 0.1). Difference electron-density maps

Table 2
Refinement statistics.

'Full' corresponds to sites with unit occupancy and 'partial' to sites with occupancy less than one.

Resolution range (Å)	10.0–0.82
No. of reflections	282465
R_{free}/R_{work} [$F_o > 4\sigma(F_o)$] (%)	11.05/9.71
R_{free}/R_{work} (all data) (%)	11.28/9.93
No. of reflections [$F_o > 4\sigma(F_o)$]	265803
$R1$† for $F_o > 4\sigma(F_o)$ (%)	9.73
$R1$† for all data (%)	9.95
No. of parameters	32154
No. of refined non-H sites	
Total (full/partial)	2087/1222
Protein (full/partial)	1968/1033
Cofactor (full/partial)	4/0
Water (full/partial)	383/142
Citrate (full/partial)	0/39
R.m.s. deviations from ideal values	
Bond distances (Å)	0.017
Angle distances (Å)	0.020
Planar groups (Å)	0.406
DELU (Å^2)	0.006
SIMU (Å^2)	0.033
ISOR (Å^2)	0.084
Average isotropic B factors	
Protein (full/partial) (Å^2)	7.5/12.1
Cofactor (full/partial) (Å^2)	5.6/—
Water (full/partial) (Å^2)	20.3/15.7
Citrate (full/partial) (Å^2)	—/12.4
Average coordinate uncertainties	
Protein (full/partial) (Å)	0.011/0.059
Cofactor (full/partial) (Å)	0.007/—
Water (full/partial) (Å)	0.032/0.041
Citrate (full/partial) (Å)	—/0.046

† $R1 = \sum \left| |F_o| - |F_c| \right| / \sum |F_o|$.

calculated from the resulting model are shown in Fig. 4. Figures were prepared with *PyMOL* (http://www.pymol.org).

3. Results and discussion

3.1. Quality of the model

The agreement of the model with the data is excellent, as evidenced by the low crystallographic R values [R_{free} = 11.1% and R_{work} = 9.7% for $F_o > 4\sigma(F_o)$]. The model contains 315 residues (of the 316 present in the construct used for crystallization), the cofactor NADP$^+$, two citrate molecules and 525 water sites. The protein is described by 1968 fully occupied and 1033 partially occupied sites, while in the solvent region 383 fully occupied and 142 partially occupied sites have been modelled. The cofactor is fully ordered. One of the citrate molecules is fully occupied and located on the surface of the protein close to Gln49, Glu53, Asp98 and Lys94; the other is present in two conformations in the active site.

All dihedral angles of the protein backbone fall in the allowed (89.5%) and additionally allowed (10.5%) regions of the Ramachandran plot as defined in the program *PROCHECK* (Laskowski *et al.*, 1993). The mean B values for the fully and partially occupied sites of the protein are 7.5 and 12.1 Å^2, respectively. The mean estimated coordinate uncertainty for fully occupied atomic sites is 0.011 Å (Table 2).

3.2. Description of the structure

The overall structure of human aldose reductase (AR) is identical to the previously determined structures of the molecule. The cofactor is bound to the protein and the active site contains citrate and several water molecules. In comparison to the recently determined structure of the AR–citrate complex at 1.4 Å resolution (El-Kabbani, Darmanin *et al.*, 2004), the higher resolution of the diffraction data in the present study (0.82 Å) allowed the refinement of anisotropic displacement parameters and the modelling of a number of residues in more than one conformation. About 28% of all residues have been modelled in more than one conformation (89 of 315). The more detailed description of the crystal structure allowed a significant improvement in terms of the R values (R_{free} = 18.4% compared with 10.9%) and mean coordinate uncertainties ($\sim$0.07 Å compared with $\sim$0.01 Å).

The high-quality electron-density maps showed all the H atoms of the cofactor. In particular, in the vicinity of the C18 atom only a single peak of electron density was found in the plane of the nicotinamide moiety, allowing unequivocal identification of the redox state of the cofactor as NADP$^+$ (Fig. 5).

3.3. The active site

The active site can be divided into a rigid region termed the 'anion-binding pocket' (residues Trp20, Val47, Tyr48, Trp79 and His110) and a more flexible part termed the the 'specificity pocket' (residues Thr113, Phe115, Phe122, Cys303 and Tyr309) which undergoes conformational changes to accommodate different ligands (Urzhumtsev *et al.*, 1997; Harrison *et*

al., 1994; Klebe *et al.*, 2004; Sotriffer *et al.*, 2004). A third set of residues (Val297–Leu300) has also been found to be capable of movement when interacting with certain ligands such as IDD594 (Podjarny *et al.*, 2004), tolrestat (Urzhumtsev *et al.*, 1997) or zenarestat (Kinoshita *et al.*, 2002).

Although the crystals used in this study were obtained by incubating the protein with the cofactor and the 2R4R stereoisomer of the inhibitor Fidarestat (El-Kabbani, Darmanin *et al.*, 2004), we were not able to model the difference electron density present in the active site by the placement of fully or partially occupied copies of the inhibitor molecule. After careful inspection, we decided to model the density as two overlapping partial conformations of citrate (which was present in the crystallization buffer), leading to a satisfactory explanation of all peaks in the difference electron density (Fig. 3).

As in many previously determined structures (Borhani *et al.*, 1992; Harrison *et al.*, 1994, 1997; Calderone *et al.*, 2000; Kinoshita *et al.*, 2002; Wilson *et al.*, 1993; El-Kabbani, Darmanin *et al.*, 2004; Ehrig *et al.*, 1994; El-Kabbani *et al.*, 2003; Howard *et al.*, 2004; Wilson *et al.*, 1992; Ruiz *et al.*, 2004; Singh *et al.*, 2006), Tyr48 and His110 interact with a carboxylate group of the ligand. Both conformations of the citrate molecule are in fact anchored to the active site *via* hydrogen bonds to Tyr48 and His110 (Table 3 and Fig. 6b). In addition to these strong interactions, the minor conformation of the ligand interacts only weakly with the protein *via* a π-hydrogen bond between O3 and the indole of Trp20, while the remaining carboxylate functions are saturated by hydrogen bonds to water molecules. In contrast to the minor conformation, the major conformation of the citrate molecule engages in a number of interactions connecting different parts of the active site. The carboxylate group that connects to Tyr48 and His110
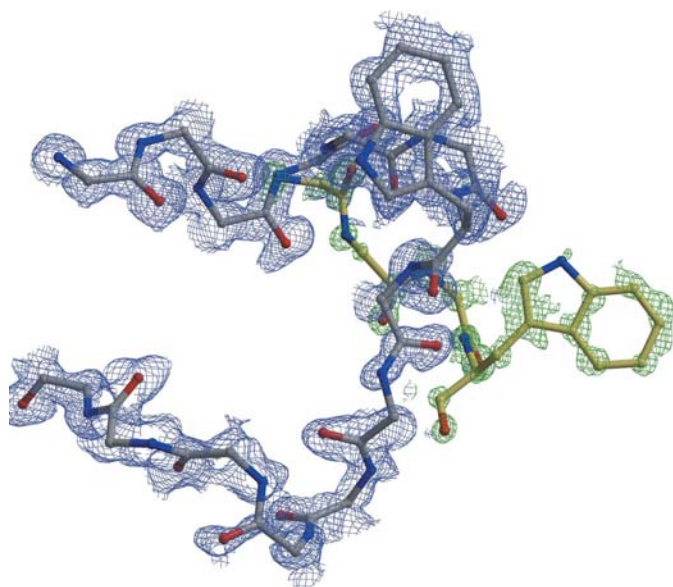

Figure 4
Electron-density map for the safety-belt loop. Residues Gly213–Leu227 of the major conformation are shown in grey; residues Asp216–Trp219 of the minor conformation are shown in yellow. The σ_A-weighted $2mF_o - DF_c$ difference electron density contoured at 1σ and the $F_o - F_c$ difference electron density contoured at 2σ (after omitting the minor conformation from the model, see §2 for details) are plotted in blue and green.
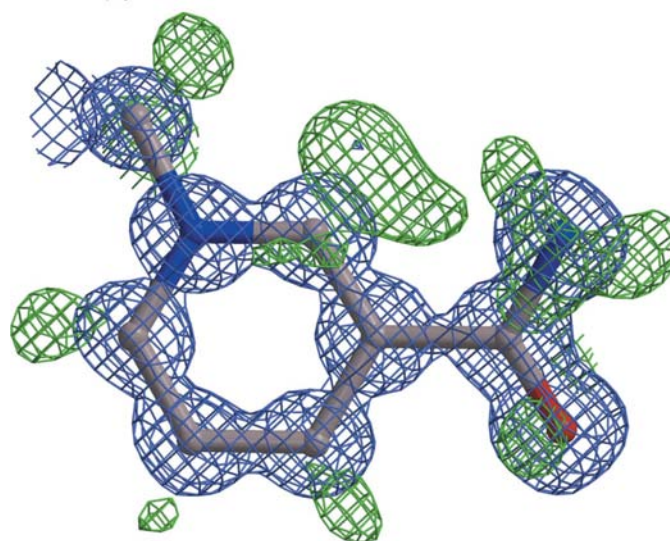

Figure 5
Electron density for the nicotinamide moiety of the cofactor. σ_A-Weighted $2mF_o - DF_c$ difference electron density contoured at 1σ (in blue) and $F_o - F_c$ difference electron density contoured at 2σ (in green) are shown. The difference density clearly shows the H atoms that had not been included in the structure-factor calculation.

also forms a hydrogen bond to the indole N atom of Trp111. The carboxylate group containing O5 and O6 of the citrate molecule acts as a bridge between Trp20 (hydrogen bond between O5 and Trp20 NE1) and Trp219 of the safety-belt loop. The latter interaction between O6 and Trp219 is characterized by the O6 atom being located in the plane of the indole of Trp219 (at an elevation of 0.21 Å above the plane fitted to the indole atoms) at a distance of 4.41 Å from the centre of mass of the six-membered ring of indole, indicating an interaction between O6 and the edge of the aromatic system. The geometry of this interaction is in excellent agreement with the results of quantum-mechanical calculations for the interaction between oxygen and the edge of benzene (Thomas *et al.*, 1982) and statistical analyses of protein structures (Hakansson, 1996).

3.4. The safety belt

In correlation with the two conformations of citrate in the active site, the safety-belt loop is also present in two conformations. In fact, in the refinement the occupancies of all sites involved were modelled using a single parameter as described by one 'free variable' in the *SHELXL* framework (Sheldrick & Schneider, 1997). For the major conformation, the entire polypeptide chain between Gly213 and Ser226 could be placed into electron density, although for residues Asp216–Asp224 the atomic sites are only partially occupied. The structure of this conformation of the safety belt corresponds to the closed conformation that is present in most of the structures of the holoenzyme, including the characteristic hydrogen bonds between the carboxylate of Asp216 and the amino groups of Lys21 and Lys262 (Wilson *et al.*, 1992) with lengths of 2.95 and 2.82 Å, respectively. For the minor conformation (37% occupancy), only residues Asp216–Trp219 are visible in the electron density (Fig. 4). The positional stability of this part of the minor conformation is mainly a consequence of interactions between Pro218 and Trp219 with Asn256 of a symmetry-

Table 3
Interactions between citrate and protein.

Cit-A and Cit-B stand for the major and the minor conformation of the citrate molecule located in the active site of human AR.

Cit-A			Cit-B		
Atom	Atom	Distance (Å)	Atom	Atom	Distance (Å)
O1	WAT	2.76	O1	n/a	—
O2	WAT	3.07	O2	n/a	—
O3	Tyr48 OH	3.14	O3	Trp20†	3.28
	His110 NE2	2.81			
O4	Trp111 NE1	2.99	O4	Tyr48 OH	2.71
				His110 NE2	2.72
O5	WAT	2.26	O5	WAT	2.30
O6	Trp219‡	4.41	O6	WAT	2.34
O7	n/a	—	O7	n/a	—

† For Cit-B O3, the distance given is the distance to the least-squares plane through the indole ring of Trp20.   ‡ For Cit-A O6, the distance given corresponds to the distance to the centre of mass of the six-membered ring of the indole moiety of Trp219.

related molecule: Pro218 forms a hydrogen bond with its carbonyl O atom to the amide N atom of the Asn256 side chain, while the indole of Trp219 engages in π-stacking interactions with the same amide group of Asn256. In terms of opening of the safety belt, the minor conformation seen here corresponds to an intermediate conformation between the closed and the open conformation as observed by Bohren *et al.* (1994), as residues Gly213–Pro215 remain in the closed conformation and the region between Ala220 and Ser226 is disordered (Fig. 2).

When we compared the modelling of the safety-belt loop in this model refined at atomic resolution with models constructed against lower resolution diffraction data, it became apparent that in other crystal structures of aldose reductase the safety loop may also have been partly disordered, as the *B* values for atoms in the region between Gly213 and Ser226 are elevated [*e.g.* for PDB entry 1ads (Wilson *et al.*, 1992) or for PDB entries 2acs and 2acr (Harrison *et al.*, 1994)].
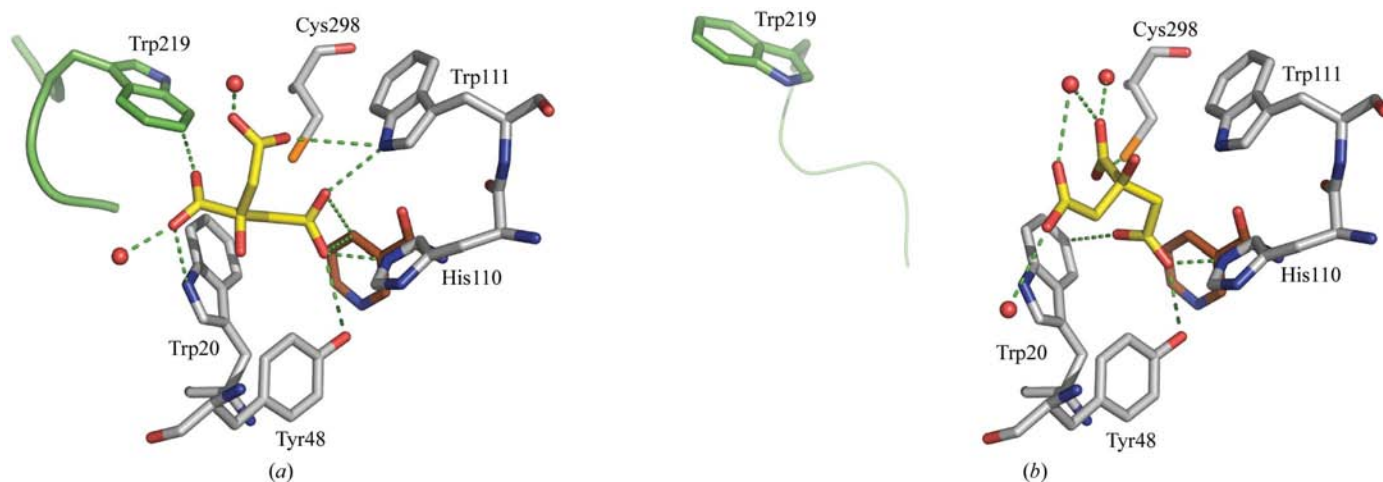

Figure 6
Interactions of the citrate molecule (in yellow) in the active site. Residues belonging to the protein are shown in grey (green for the safety belt); the nicotinamide moiety is coloured orange. (*a*) and (*b*) show the major and the minor conformation of the citrate, respectively.

4. Conclusions and perspectives

We have presented a substantially improved model of the crystal structure of AR in complex with citrate. For the atomic resolution data, the agreement between the model and the data was significantly improved with respect to the previously determined structure of the same complex (El-Kabbani, Darmanin *et al.*, 2004). A larger number of residues were modelled in multiple conformations than in the previously determined structure (89 compared with 47). Notably, these multiple conformations include two discrete conformations of the safety-belt loop, the part of the molecule responsible for uptake and release of the cofactor.

As evident from the H atoms present on the nicotinamide moiety of the cofactor, the cofactor is in its oxidized state. Therefore, the holoenzyme in the present crystal structure is in a state corresponding to the situation after catalysis is completed and the safety belt should have opened to release the cofactor. In the crystals used in this study, the safety-belt loop in a major fraction of the molecules (63%) is kept in a closed conformation by a citrate molecule that connects Trp219 to residues of the active site, some of which (Tyr48 and His110) are known to be very rigidly placed. For the remaining 37% of the molecules in the crystal, the citrate assumes a conformation that does not engage in an interaction with Trp219. This conformation of the citrate correlates with a 'half-open' conformation of the safety-belt loop, indicating that small adjustments of a ligand in the active site can suffice to trigger release of the cofactor. Such a transition from a situation where the safety belt is held closed by interactions with substrate or product to a situation where the safety belt can open after important interactions cannot be maintained after the reorientation of the product could well be the structural basis of the regulation of cofactor release.

In the context of drug design, the present study shows that Trp219 in the safety belt in its closed conformation provides a key interaction point for ligands. Exploiting this interaction point in the construction of ligands for aldose reductase may enable both the affinity and the specificity of potential drugs to be increased.

References

Bohren, K. M., Brownlee, J. M., Milne, A. C., Gabbay, K. H. & Harrison, D. H. (2005). *Biochim. Biophys. Acta*, **1748**, 201–212.

Bohren, K. M., Grimshaw, C. E., Lai, C. J., Harrison, D. H., Ringe, D., Petsko, G. A. & Gabbay, K. H. (1994). *Biochemistry*, **33**, 2021–2032.

Borhani, D. W., Harter, T. M. & Petrash, J. M. (1992). *J. Biol. Chem.* **267**, 24841–24847.

Calderone, V., Chevrier, B., Van Zandt, M., Lamour, V., Howard, E., Poterszman, A., Barth, P., Mitschler, A., Lu, J., Dvornik, D. M., Klebe, G., Kraemer, O., Moorman, A. R., Moras, D. & Podjarny, A. (2000). *Acta Cryst.* D**56**, 536–540.

Costantino, L., Rastelli, G., Cignarella, G. & Barlocco, D. (2000). *Farmaco*, **55**, 544–552.

Costantino, L., Rastelli, G., Vianello, P., Cignarella, G. & Barlocco, D. (1999). *Med. Res. Rev.* **19**, 3–23.

Dunlop, M. (2000). *Kidney Int. Suppl.* **77**, S3-12.

Ehrig, T., Bohren, K. M., Prendergast, F. G. & Gabbay, K. H. (1994). *Biochemistry*, **33**, 7157–7165.

El-Kabbani, O., Darmanin, C., Schneider, T. R., Hazemann, I., Ruiz, F., Oka, M., Joachimiak, A., Schulze-Briese, C., Tomizaki, T., Mitschler, A. & Podjarny, A. (2004). *Proteins*, **55**, 805–813.

El-Kabbani, O., Ramsland, P., Darmanin, C., Chung, R. P. & Podjarny, A. (2003). *Proteins*, **50**, 230–238.

El-Kabbani, O., Ruiz, F., Darmanin, C. & Chung, R. P. (2004). *Cell. Mol. Life Sci.* **61**, 750–762.

Grimshaw, C. E., Bohren, K. M., Lai, C. J. & Gabbay, K. H. (1995). *Biochemistry*, **34**, 14356–14365.

Grimshaw, C. E., Shahbaz, M. & Putney, C. G. (1990a). *Biochemistry*, **29**, 9936–9946.

Grimshaw, C. E., Shahbaz, M. & Putney, C. G. (1990b). *Biochemistry*, **29**, 9947–9955.

Hakansson, K. (1996). *Int. J. Biol. Macromol.* **18**, 189–194.

Harrison, D. H., Bohren, K. M., Petsko, G. A., Ringe, D. & Gabbay, K. H. (1997). *Biochemistry*, **36**, 16134–16140.

Harrison, D. H., Bohren, K. M., Ringe, D., Petsko, G. A. & Gabbay, K. H. (1994). *Biochemistry*, **33**, 2011–2020.

Howard, E. I., Sanishvili, R., Cachau, R. E., Mitschler, A., Chevrier, B., Barth, P., Lamour, V., Van Zandt, M., Sibley, E., Bon, C., Moras, D., Schneider, T. R., Joachimiak, A. & Podjarny, A. (2004). *Proteins*, **55**, 792–804.

Kinoshita, J. H. & Nishimura, C. (1988). *Diabetes Metab. Rev.* **4**, 323–337.

Kinoshita, T., Miyake, H., Fujii, T., Takakura, S. & Goto, T. (2002). *Acta Cryst.* D**58**, 622–626.

Kissinger, C. R., Gehlhaar, D. K. & Fogel, D. B. (1999). *Acta Cryst.* D**55**, 484–491.

Klebe, G., Kramer, O. & Sotriffer, C. (2004). *Cell. Mol. Life Sci.* **61**, 783–793.

Kubiseski, T. J., Hyndman, D. J., Morjana, N. A. & Flynn, T. G. (1992). *J. Biol. Chem.* **267**, 6510–6517.

Lamour, V., Barth, P., Rogniaux, H., Poterszman, A., Howard, E., Mitschler, A., Van Dorsselaer, A., Podjarny, A. & Moras, D. (1999). *Acta Cryst.* D**55**, 721–723.

Laskowski, R. A., Moss, D. S. & Thornton, J. M. (1993). *J. Mol. Biol.* **231**, 1049–1067.

McRee, D. E. (1999). *J. Struct. Biol.* **125**, 156–165.

Otwinowski, Z. & Minor, W. (1997). *Methods Enzymol.* **276**, 307–326.

Pavelites, J., Gao, J., Bash, P. A. & MacKerell, A. D. J. (1997). *J. Comput. Chem.* **18**, 221–239.

Petrash, J. M. (2004). *Cell. Mol. Life Sci.* **61**, 737–749.

Podjarny, A., Cachau, R. E., Schneider, T., Van Zandt, M. & Joachimiak, A. (2004). *Cell. Mol. Life Sci.* **61**, 763–773.

Rondeau, J. M., Tete-Favier, F., Podjarny, A., Reymann, J. M., Barth, P., Biellmann, J. F. & Moras, D. (1992). *Nature (London)*, **355**, 469–472.

Rosenbaum, G., Alkire, R. W., Evans, G., Rotella, F. J., Lazarski, K., Zhang, R. G., Ginell, S. L., Duke, N., Naday, I., Lazarz, J., Molitsky, M. J., Keefe, L., Gonczy, J., Rock, L., Sanishvili, R., Walsh, M. A., Westbrook, E. & Joachimiak, A. (2006). *J. Synchrotron Rad.* **13**, 30–45.

Rossi, M., Rickles, L. F. & Glusker, J. P. (1983). *Acta Cryst.* C**39**, 987–990.

Ruiz, F., Hazemann, I., Mitschler, A., Joachimiak, A., Schneider, T., Karplus, M. & Podjarny, A. (2004). *Acta Cryst.* D**60**, 1347–1354.

Sheldrick, G. M. & Schneider, T. R. (1997). *Methods Enzymol.* **277**, 319–343.

Singh, R., White, M. A., Ramana, K. V., Petrash, J. M., Watowich, S. J., Bhatnagar, A. & Srivastava, S. K. (2006). *Proteins*, **64**, 101–110.

Sotriffer, C. A., Kramer, O. & Klebe, G. (2004). *Proteins*, **56**, 52–66.

Srivastava, S. K., Ramana, K. V. & Bhatnagar, A. (2005). *Endocr. Rev.* **26**, 380–392.

Thomas, K. A., Smith, G. M., Thomas, T. B. & Feldmann, R. J. (1982). *Proc. Natl Acad. Sci. USA*, **79**, 4843–4847.

Urzhumtsev, A., Tete-Favier, F., Mitschler, A., Barbanton, J., Barth, P., Urzhumtseva, L., Biellmann, J. F., Podjarny, A. & Moras, D. (1997). *Structure*, **5**, 601–612.

Wilson, D. K., Bohren, K. M., Gabbay, K. H. & Quiocho, F. A. (1992). *Science*, **257**, 81–84.

Wilson, D. K., Tarle, I., Petrash, J. M. & Quiocho, F. A. (1993). *Proc. Natl Acad. Sci. USA*, **90**, 9847–9851.

Yabe-Nishimura, C. (1998). *Pharmacol. Rev.* **50**, 21–33.